Experimental Study on Cathodic Protection of Anchor Bar

Jiangong Chen, Jingrui Xu*, Xiaoyu Ma, Ziyi Wu

School of Civil Engineering, Chongqing University, Chongqing 400045, China

*E-mail: 202316021065@stu.cqu.edu.cn

Abstract. A self-designed cathodic protection (CP) setup with an externally applied current was developed, using a copper wire ring buried in the soil layer, aligned with the anchor rod axis, as the anode, and the anchor rod as the cathode, connected to a DC power supply to form a current loop, to achieve rust prevention for the anchor bar. Indoor simulation experiments are conducted to analyze the distribution of electric fields and the degree of corrosion of the anchor bar under different voltages, copper wire ring diameters, and anchor bar lengths. The results show that the anchor bar with the externally applied cathodic protection effectively slows down its corrosion process compared to the anchor bar without cathodic protection. A larger diameter of the anode copper wire ring results in less corrosion. An increase in the length of the anchor bar leads to a decrease in the surface potential along the depth direction, affecting the protective effect. The minimum protective potential on the surface of the anchor rod is 760-820mV.

Keywords: Anchor Corrosion Protection; Cathodic Protection; The minimum protective potential for the anchor bar

1 Introduction

Anchor bars have received wide attention in the geotechnical engineering field and have been widely used in various areas such as foundation pits and tunnel rock support. However, once affected by groundwater, internal temperature, and the composition of soil and rock, the anchor bars can corrode, posing a significant threat to engineering safety. Therefore, research on corrosion protection for anchor bars is particularly urgent. Over the years, scholars have conducted extensive research on corrosion protection for anchor bars. Cathodic Protection (CP), as an effective corrosion protection method, involves applying an external electric current to the metal structure's surface to turn it into a cathode, thus slowing down the metal corrosion process [1, 2]. Since Davy first applied CP to combat metal corrosion in the UK 200 years ago, scholars worldwide have extensively researched and applied this method [3, 4]. The development of this technology, from German scholars Bauer and Vogel studying CP for iron and low-carbon steel in the soil to the application of CP technology in protecting steel reinforcements in concrete in the 1950s, and the widespread use of cathodic protection

G. Zhao et al. (eds.), *Proceedings of the 2024 7th International Symposium on Traffic Transportation and Civil Architecture (ISTTCA 2024)*, Advances in Engineering Research 241,
https://doi.org/10.2991/978-94-6463-514-0_68

for steel structures in soil in the early 20th century, reflects humanity's relentless efforts against corrosion [5]. Researchers like Ni Meng have studied the distribution patterns of electric potential around long-distance pipelines using mathematical models and theoretical analysis, exploring the impact of complex environments and different anode conditions on pipeline potential distribution [6]. Jia Liwen and their team have applied cathodic protection to protect structures against corrosion and conducted corrosion fatigue tests, studying the effects of different potentials on structural fatigue crack formation [7]. Cui Zhen has optimized the design of cathodic protection devices for long-distance pipelines, controlling the pipeline potential within a certain range [8]. The photoelectrochemical cathodic protection technology proposed by Yuan and Tsujikawa in 1995, along with Federico and others combining existing theories to propose a new cathodic protection mechanism for steel in a porous medium, have made significant contributions to this field's advancement [9-11].

This study aims to investigate the corrosion of metal anchor bars under the influence of external currents. By studying the patterns of the electric field distribution around metal anchor bars, one can analyze both the electric field within the anchoring mortar and the surface potential distribution of the anchor bars. Utilizing variable control methods, researchers can adjust the external voltage, anode ring radius, and anchor bar length to summarize the relationships between potential, voltage, anode ring radius, and burial depth variations. Ultimately, this process will lead to the determination of the minimum protective potential necessary for the cathodic protection of anchor bars. By using cathodic protection with external currents to prevent corrosion of anchor bars (cables) deeply buried in rock and soil layers, the aim is to extend the service life of anchor bars (cables), reduce the risk of their failure, and decrease the costs of maintenance and replacement. This not only serves as an important supplement to existing corrosion protection technologies but also represents a beneficial exploration in the field of anchor bar corrosion research.

2 Experimental Setup for Cathodic Protection of Anchor Bar

The experimental setup for cathodic protection of the anchor bar is shown in Fig. 1. Cement mortar is poured into the corrugated pipe, with the anchor bar placed at the center of the corrugated pipe and the copper wire ring placed on the surface of the cement mortar. An adjustable DC-regulated power supply is used to provide stable current, with the anchor bar connected to the negative pole of the power supply and the copper wire ring connected to the positive pole of the power supply, so that the current flows out from the positive electrode of the power supply, enters the cement mortar through copper wire ring, then flows to the surface of the anchor bar, and finally returns to the negative electrode of the power supply. To study the distribution of electric fields in the anchor bar-cement mortar system, two nails are inserted into the surface of the cement mortar to measure the grounding resistance of the anchor bar. The measuring points 1~ 4 are embedded in the mortar 75mm away from the surface of the anchor bar, measuring the potential of the points after power-on, along with measuring the total current and voltage values. The corrugated pipe is filled with water to saturate the

cement mortar, simulating a compared environment as shown in Fig. 2.

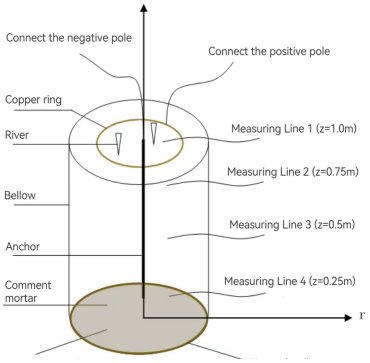

Fig. 1. Diagram of the experimental setup

Fig. 2. Top view of the experimental device.

2.1 Measurement of the Corrosion Level of Anchor Bar

Rust is an oxide compound formed by the combination of oxygen and iron, with a lower electrical conductivity compared to iron. As the anchor bar undergoes oxidation and rusting, the resistance gradually increases [12]. Therefore, changes in the grounding resistance value can reflect the extent of rusting on the anchor bar. This experiment utilizes two methods to measure the changes in the anchor bar's resistance. Firstly, by calculating the total resistance value R0=U0/I0 using the total current value I0 and voltage value U0 monitored by the DC stabilized power supply equipment to reflect the overall rusting situation of the system. Secondly, by using a clamp-on earth resistance tester to measure the earth resistance value RA of the anchor bar to reflect the rusting situation of the anchor bar.

2.2 Measurement of Electric Field Strength at Measurement Points

Measure the voltage between 4 internal points in the mortar, namely the measurement line elect-bares and the cathode end (anchor bar end). Connect the gilded test probe to

the multimeter, with one end of the probe touching the positive terminal of the power supply, and the other end sequentially touching the measurement line elect-bares to record the voltage ΔU at each measurement point. This allows for the calculation of the electric field strength E at that point, and subsequently the calculation of the average current density J at that point.

3 Testing Schemes

In the experimental setup, the voltage, copper wire ring radius, and steel bar length of the anchor bar have a significant impact on the distribution pattern of the electric field. The experiment includes a total of four control groups as shown in Table 1.

Control group 1 consists of three specimens, Specimen 1, Specimen 2, and Specimen 3. The study investigates the electric field by varying the voltage. The initial voltage of the three specimens is set at 15V, with the voltage changing every 8 days, decreasing by 1V each time, until after 120 days, the voltage drops from 15V to 1V. The anchor bar is buried at a depth of 0.75m, and the radius of the copper wire ring is 0.125m.

Control group 2 consists of three specimens, Specimen 4, Specimen 5, and Specimen 6. The study explores the impact of varying the radius of the copper wire ring on the electric field distribution. The radius of the copper wire ring is 0.125m for Specimen 4, 0.1m for Specimen 5, and 0.075m for Specimen 6. The anchor bars for these three specimens are buried at a depth of 0.75m, with the initial voltage set at 6V.

Control group 3 comprises three specimens, Specimen 7, Specimen 8, and Specimen 9. The study examines the influence of varying the depth of the anchor bar on the distribution of the electric field. Specimen 7 has an anchor bar depth of 0.75m, Specimen 8 has a depth of 0.7m, and Specimen 9 has a depth of 0.65m. The specimens in this group have a copper wire ring radius of 0.125m, with the initial voltage set at 6V, to avoid ineffective experiments caused by high voltage on anchor bar protection.

Control group 4 consists of one specimen, Specimen 10. Specimen 10 lacks any corrosion protection measures, and the anchor bar corrodes spontaneously in cement mortar. By measuring the earth resistance of Specimen 10 and comparing it with the earth resistance of the other three control groups.

Table 1. Experimental control group.

Control group	Specimen number	Voltage (V)	Copper ring radius (m)	Anchor length (m)
Control group 1	Specimen No.1	15→1	0.125	0.75
	Specimen No.2	15→1	0.125	0.75
	Specimen No.3	15→1	0.125	0.75
Control	Specimen No.4	6	0.125	0.75

group 2	Specimen No.5	6	0.1	0.75
	Specimen No.6	6	0.075	0.75
Control group 3	Specimen No.7	6	0.125	0.75
	Specimen No.8	6	0.125	0.7
	Specimen No.9	6	0.125	0.65
Control group 4	Specimen No.10	—	0.125	0.75

4 Experimental Results and Analysis

4.1 Test Results for Control Group 1

The Potential of the Measurement Point Changes with the Applied Voltage.

Fig. 3 compares the results of Specimen 1, 2, and 3 from control group 1 under identical conditions. During the experiment, the voltage applied to the copper ring was varied from 15V down to 1V, while the radius of the copper ring was 0.125m and the length of the anchor was 0.75m. The voltage was adjusted every 8 days. The potential graphs depicting the comparative experimental measurements of control group 1 capture the fluctuations in potentials at the four measurement points as the voltage gradually decreases from 15V to 1V over 120 days for test Specimens 1, 2, and 3. The trend in the variation of point potential was consistent among all three experimental Specimens. The steepest decrease in potential was observed at measured point 1, followed by measured point 2, measured point 3, and lastly, measured point 4. The potential change trend is consistent across the three Specimens, all exhibiting a gradual decline like stairs. At identical voltages, the potential of each measuring point fluctuates within a fixed range.

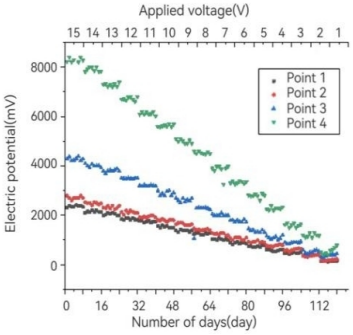

(a) Specimen 1 test point potential map

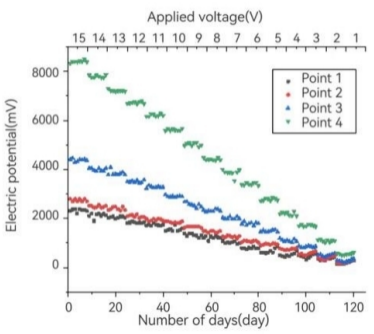

(b) Specimen 2 test point potential map

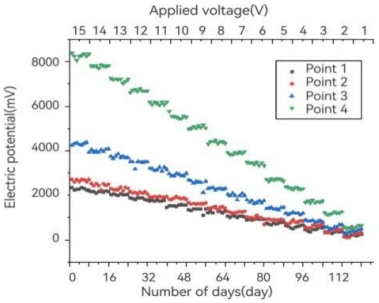

(c) Specimen 3 test point potential map

Fig. 3. Control group 1 experimental measuring point potential diagram.

Fig. 3, shown as the potential measurement charts of control group 1 compared the changes in potential at 4 measurement points of specimens 1, 2, and 3 as the voltage decreased from 15V to 1V over 120 days under the same conditions. During the experiment, with a copper wire ring radius of 0.125m and anchor bar length of 0.75m, the external voltage applied to the copper wire ring was decreased from 15V to 1V, with the voltage changed every 8 days. It can be observed that the potential changes of the measuring points in the three experimental specimens show a similar trend, with the rate of potential decrease being measuring point 1 > point 2 > point 3 > point 4. The potential changes in the three specimens show a consistent trend, all exhibiting a stepwise decrease, where at the same voltage, the potential of the same measuring point fluctuates around a fixed value.

Variation of Anchor Bar Earth Resistance with Applied Voltage.

Fig. 4 shows the curve of the grounding resistance of specimens 1, 2, and 3 in control group 1. During the process from the first day to the 80th day of the experiment, as the applied voltage dropped from 15V to around 6V, the earth resistance of the anchor bars remained almost unchanged, stabilizing at around 10Ω. As the applied voltage decreased to 5V, the rate of increase in the earth resistance of the anchor bars gradually increased, reaching approximately 12.1Ω at 5V. When the applied voltage dropped to 1V, the grounding resistance of the anchor bars was 23.5Ω. The gradual increase in grounding resistance after the applied voltage dropped to 5V indicates that the anchor bars are beginning to corrode, with the resistance of the rust substance being 3 to 6 times greater than that of the anchor bars themselves, leading to an increase in the measured earth resistance value. When the applied voltage is 6V, the potential change range of measurement point 4 is 800~900mV. Therefore, the protection voltage within the system is 6V, and the protective potential of measurement point 4 is greater than 800mV.

At 6V, the anchor did not corrode. Yet, as the voltage dipped to a mere 5V, the anchor succumbed to the ravages of corrosion. Therefore, the critical voltage for the anchor not to compare is 6V. The critical value of the protective potential of measuring point 4 corresponds to the potential value of measuring point 4 in the range of 5V to 6V.

Table 2 below shows the potential values for an applied voltage of 6V (3 values) and 5V (4 values):

When the external voltage is 6V, the anchor bar does not compare. However, when the external voltage drops to 5V, the anchor bar starts to rust. Therefore, 6V is the critical external voltage threshold for the anchor bar to remain corrosion-free. The potential value at measurement point 4 corresponding to the external voltages between 5V and 6V represents the critical protection potential value at measurement point 4, as shown in Table 2.

Table 2. The potential critical value of measuring point 4.

Specimens	6V			5V			
Specimen 1	903.50	813.53	870.48	747.74	764.65	727.21	704.65
Specimen 2	853.02	797.42	848.09	822.8	696.76	789.43	742.57
Specimen 3	834.58	833.38	820.43	747.69	804.6	693.78	744.6

Comparison with Anchor Bars without Anticorrosion Measures.

Fig. 5 shows a comparison graph of the anchor earth resistance between control group 1 and control group 4. It is evident from the graph that there is a noticeable difference in earth resistance between cathodic protection with external current and without any corrosion protection measures. The earth resistance of Specimen 10 has been steadily increasing since the beginning of the experiment, rising from 10Ω to 60Ω before stabilizing. The experiment indicates that without external voltage, the earth resistance of the anchor bar is six times its resistance value after corrosion. Once it reaches six times, the corrosion products cease to increase, and the grounding resistance value stabilizes.

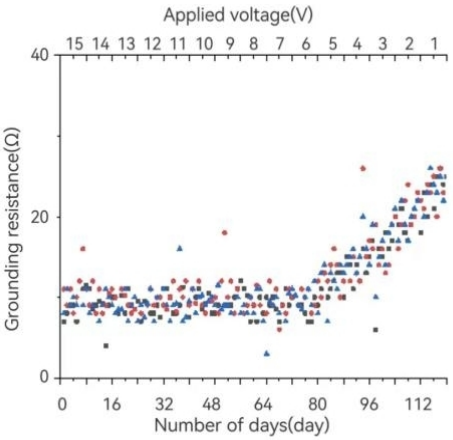

Fig. 4. Distribution diagram of grounding resistance under different applied voltages.

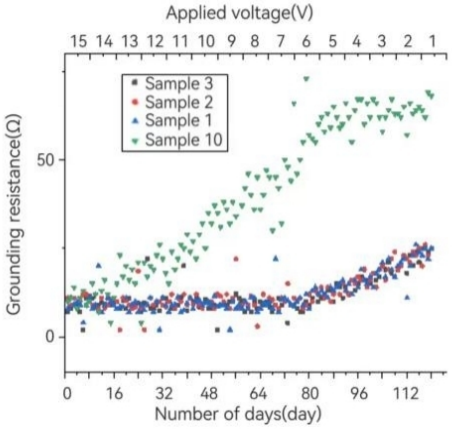

Fig. 5. Changes in grounding resistance of anchor bars in control group 1 and control group 4.

Fig. 6a shows the image of specimen 10 after ten days of the experiment. It is visible that the rust substance has appeared on the surface of the anchor bar, indicating corrosion. In contrast, Fig. 6b shows specimen 1 with a smooth surface, and almost no rust formation, indicating that the anchor bar is protected under the influence of external voltage and has not undergone corrosion.

As depicted in Fig. 6a, the image displays the anchor bar of Specimen 10 after ten days of the experiment. A layer of rust has formed on the surface of the anchor bar, signifying the occurrence of corrosion. However, as illustrated in Fig. 6b, Specimen 1 reveals a smooth surface of the anchor bar with minimal rust formation, suggesting that the anchor bar is shielded from corrosion by the protection of the applied voltage.

(a) Anchor without applied voltage (b) With the addition of voltage anchor

Fig. 6. Comparison of anchor bars with and without protection measures.

4.2 Test results for Control Group 2

Impact of Copper Wire Ring Radius on Potentials.

Fig. 7 shows the experimental results of Control Group 2, where Specimen 4,

Specimen 5, and Specimen 6 are subjected to a voltage of 6V with an anchor bar length of 0.75m. The copper wire ring radius is 0.125m for Specimen 4, 0.1m for Specimen 5, and 0.075m for Specimen 6. It can be observed from the graph that the potentials at each measurement point tend to stabilize under the same applied voltage. The distribution of the electric field in the component gradually decreases with increasing depth. As the radius of the copper wire ring decreases, the potential at the upper part of the specimen increases while the potential at the lower part decreases, indicating a significant impact of the copper wire ring size on the depth range of the electric field effect.

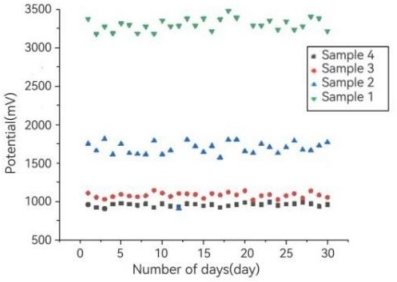

(a) Potential map of the test point of Specimen 4 (r = 0.125 m)

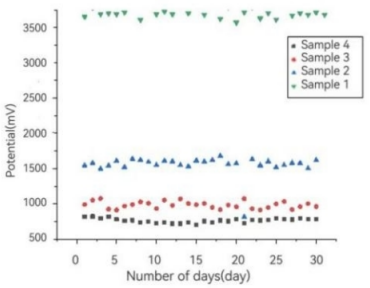

(b) Potential map of the test point of Specimen 5 (r = 0.1 m)

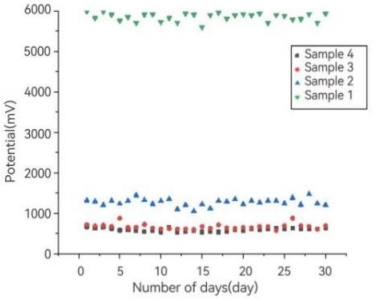

(c) Potential map of test point of Specimen 6 (r=0.075m)

Fig. 7. Copper ring group comparison experiment measuring point potential diagram.

The Influence of the Copper Wire Ring Radius on the Earth Resistance of the Anchor Bar.

Fig. 8 illustrates the curve graphs of anchor grounding resistance for Specimens 4, 5, and 6 in Control Group 2, generated by altering the radius of the copper ring. The results indicate that the anchor grounding resistance of Specimen 6 surpasses that of Specimen 5, which in turn outperforms Specimen 4. The larger the copper ring radius, the lower the anchor grounding resistance and the lesser the extent of anchor corrosion. When the outer radius of the copper ring is 0.125m, the grounding resistance value stays nearly constant at around 10Ω, which can be approximated as a horizontal straight

line. With the outer radius of the copper ring set at 0.1m, the grounding resistance at measurement point 4 rises from 10Ω to 23Ω before reaching a stable state. When the outer radius of the copper ring is 0.075m, the grounding resistance at measurement point 4 climbs from 10Ω to 30Ω before leveling off. After the onset of anchor corrosion, the grounding resistance experiences a gradual incline. Around 15 days into the experiment, the resistance plateaus, ceasing to rise further. Ultimately, the grounding resistance settles at a level 2–3 times higher than that of the anchor itself.

Fig. 8 shows the earth resistance curves obtained by changing the copper wire ring radius of specimens 4, 5, and 6 in control group 2. The results indicate that the earth resistance of specimen 6 > specimen 5 > specimen 4. The larger the radius of the copper wire ring, the smaller the earth resistance of the anchor bar, and the less severe the corrosion of the anchor bar. When the radius of the copper ring is 0.125m, the earth resistance value remains almost constant at around 10Ω, forming an approximately horizontal line. When the outer radius of the copper wire ring is 0.1m, the earth resistance at measurement point 4 increases from 10Ω to 23Ω before stabilizing. When the radius of the copper wire ring is 0.075m, the grounding resistance at measurement point 4 increases from 10Ω to 30Ω before stabilizing. After the anchor bar corrodes, the earth resistance gradually increases. After about 15 days of experimentation, the resistance stabilizes, no longer increasing, with the final earth resistance value being 2 to 3 times the resistance of the anchor bar itself.

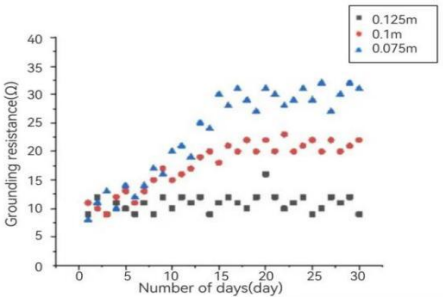

Fig. 8. Control group 2 measuring point 4 grounding resistance distribution diagram.

4.3 Test Results for Control Group 3

Influence of Anchor Bar Length on Measurement Point Potentials.

Fig. 9 shows the experimental results of control group 3. Comparative experiments were conducted on specimens 7, 8, and 9 under the same external voltage and copper wire ring radius but with different anchor bar lengths. All three specimens had an external voltage of 6V and a copper wire ring radius of 0.125m. The anchor bar lengths are 0.75m for specimen 7, 0.7m for specimen 8, and 0.65m for specimen 9. The graph illustrates that the potentials at various measurement points stabilize under the same external voltage, and the distribution of the electric field in the entire component gradually decreases with increasing depth. As the length of the anchor bar increases, the potential at each measurement point becomes smaller, which suggests that the

protective effect of the external voltage on the anchor bar is reduced. Once the anchor bar exceeds a certain length, the lower part of the anchor bar will fail to reach the minimum protective potential, leading to corrosion of the anchor bar.

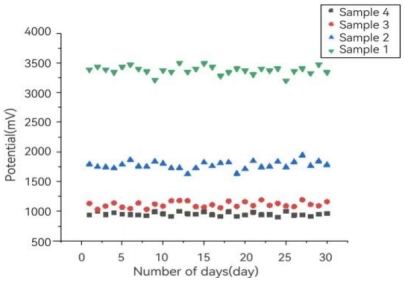

(a) Map of measurement point potentials for Specimen 7

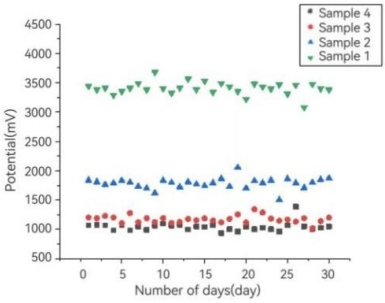

(b) Map of measurement point potentials for Specimen 8

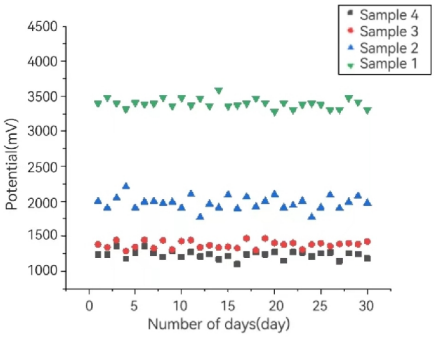

(c) Map of measurement point potentials for Specimen 9

Fig. 9. Anchor bar group comparison experiment measuring point potential diagram.

Influence of Anchor Bar Length on Earth Resistance.

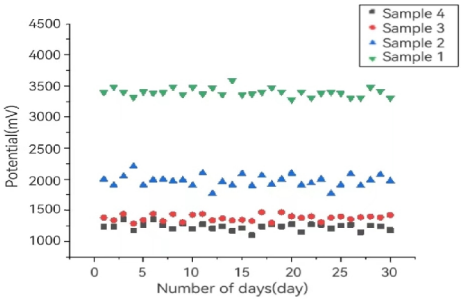

Fig. 10. Distribution of grounding resistance at measuring point 4 under different anchor lengths.

Fig. 10 shows the curve of changes in earth resistance of anchor bars for specimens 7, 8, and 9 in control group 3 with varying anchor bar lengths. The results indicate that the earth resistance values of the three specimens remained unchanged at around 10Ω, suggesting no corrosion occurred in the anchor bars.

4.4 Determining the Minimum Protective Potential of Anchor Bars

Analyzing the changes in earth resistance of the 9 specimens in Control Group 1, Control Group 2, and Control Group 3, it is observed that as the anchor bars compare, the earth resistance gradually increases. The potential at measurement point 4 at the beginning of the increase in earth resistance can be considered as the minimum protective potential. Since distinct inflection points can be found in the grounding resistance curve of the 3 specimens in Control Group 1, these 3 specimens are selected for analysis. Based on the critical potential value of measuring point 4 from Table 2, using the Shapiro-Wilk test and goodness-of-fit test in mathematical statistics, at a significance level of α=0.05, the confidence interval for the minimum protective potential Vmin at measuring point 4 is calculated to be [761.49, 815.73].

5 Conclusions

This article presents an experimental study on a self-developed experimental setup for anchor bar cathodic protection with external current. The study investigated the variations in potential at measuring points and earth resistance of the anchor bar under different conditions such as external voltage, copper wire ring radius, and anchor bar length, and determined the minimum protective potential for the anchor bar. However, it is still preliminary experimental research, and there are also some deficiencies in this study, which will need to be improved by a large number of subsequent studies such as on-site installation issues, power supply, and so on.

References

1. Sibiya, C., Kusakana, K., & Numbi, B. (2021). TRU Energy Monitoring for Potential Cost Saving in Electricity Bills for Cathodic Protection Units: South African Case. International Journal of Electrical and Electronic Engineering & Telecommunications, 145-150. https://doi.org/10.18178/ijeetc.10.2.145-150.
2. Yu, Z. (2014). Application of cathodic protection anticorrosion for metal structures. Heilongjiang Water Conservancy Science and Technology, 42(05), 173-174. https://doi.org/10.14122/j.cnki.hskj.2014.05.088.
3. Davy, H. (1824). On the Corrosion of Copper Sheeting by Sea Water, and on Methods of Preventing This Effect; And on Their Application to Ships of War and Other Ships. Philosophical Transactions of The Royal Society of London, 114, 151-158. https://doi.org/10.1098/rstl.1824.0009.
4. James, F. (1996). The appliance of science: Humphry Davy's electrochemical protectors for ships' bottoms in the 1820s. Engineering Science and Education Journal, 4, S11-S16. https://doi.org/10.1049/esej:19950615.

5. Bauer O, Vogel O. (1919). The Action of Iron Rust in Contact with Other Metals and Alloys. Scientific American Magazine. https://doi.org/DOI:10.1038/scientificamerican07121919-48.
6. Meng, N. (2019). Numerical simulation research on cathodic protection parameters of long-distance pipeline [Master's thesis, Xi'an: Xi'an Petroleum University].
7. Linan, J., Dawen, J., Yijin, S., & JI, Y. (2019). Corrosion fatigue mechanism of D36 platform steel in seawater under cathodic protection. Acoustic and Electronic Engineering(02), 46-49.
8. Zhen, C. (2019). Research on Cathodic Protection Devices for Long-Distance Pipelines [Master's thesis, Xi'an: Xi'an Petroleum University].
9. Yuan, J., Fujisawa, R., & Tsujikawa, S. (1994). Photopotentials of Copper Coated with TiO2 by Sol-Gel Method. Zairyo to Kankyo/ Corrosion Engineering, 43, 433-440. https://doi.org/10.3323/jcorr1991.43.433.
10. Yuan, J., & Tsujikawa, S. (1995). Characterization of Sol-Gel-Derived TiO[sub 2] Coatings and Their Photoeffects on Copper Substrates. Journal of The Electrochemical Society - J ELECTROCHEM SOC, 142, 3444-3450. https://doi.org/10.1149/1.2050002.
11. Martinelli-Orlando, F., Mundra, S., & Angst, U. (2024). Cathodic protection mechanism of iron and steel in porous media. Communications Materials, 5. https://doi.org/10.1038/s43246-024-00454-y.
12. Enchong, D. (2013). Exploration and protection of metal corrosion. China Education Technology Equipment(19), 144-145. https://doi.org/10.3969/j.issn.1671-489X.2013.19.144.